

# Optimized dwell time algorithm in magnetorheological finishing

Longxiang Li<sup>1,2</sup> · Ligong Zheng<sup>1</sup> · Weijie Deng<sup>1</sup> · Xu Wang<sup>1</sup> · Xiaokun Wang<sup>1</sup> · Binzhi Zhang<sup>1</sup> · Yang Bai<sup>1,2</sup> · Haixiang Hu<sup>1,2</sup> · Xuejun Zhang<sup>1</sup>

Received: 26 January 2015 / Accepted: 4 May 2015 / Published online: 14 May 2015  
© Springer-Verlag London 2015

**Abstract** An optimized dwell time algorithm for magnetorheological finishing (MRF) is discussed. Based on the D-shape of the removal function of MRF, an optimized non-negative least-squares method is introduced to get dwell time from a linear matrix equation transferred from the de-convolution operation. Moreover, one kind of general surface error map extension is developed for any shape of optics to obtain a more precise optical surface in MRF. The simulation results show that the non-negative least-squares method of the constrained generalized minimal residual (GMRES) method with adaptive Tikhonov regulation is much faster to get highly stable dwell time distribution. In combination with the general surface error map extension, the peak to valley (PV) and root mean square (RMS) of the surface error of the diameter 400 mm converge from 184.41 and 21.26 nm to 7.56 and 0.632 nm with the consistency of the edge and the aperture inside. Finally, a fabricating experiment proves the validity of the optimized algorithm. Therefore, the algorithm developed and presented in this paper can facilitate the MRF process effectively.

**Keyword** Optical fabrication · Dwell time · Linear matrix equation · Surface error map extension · Magnetorheological finishing

## 1 Introduction

Magnetorheological finishing (MRF) is one of the deterministic sub-aperture computer-controlled optical surfacing technologies, originally invented by Dr. William Kordonski and his colleagues in Belarus and commercialized by QED Technologies in the USA [1]. Its stable removal function leads to high convergence efficiency, minimizing the number of measure-polish iterations, and ultimately decreases the whole optical manufacturing time effectively. Moreover, other advantages of MRF include less sub-surface damage, fine surface roughness, and no footprint on thin optics. It is widely applied to flat, spherical, and aspherical optics in high-precision optical fabrication processes [2–7].

Just like other sub-aperture optical manufacturing technologies, the dwell time distribution is one of the key factors determining the result of MRF as shown in Fig. 1. The dwell time algorithm is based on the principle that the desired removal amounts of material on optics is a convolution operation of dwell time and removal function. With the development of the sub-aperture optical manufacturing technology, many algorithms have been established and their removal functions have usually a circular symmetrical distribution including conventional pitch lap [8], stressed lap (SL) [9], reactive atom plasma [10], and ion beam figuring (IBF) [11]. However, the special D-shape of MRF's removal function, especially for the spiral path, demands algorithms dealing with the discrete convolution model which has to be changed, such as the Fourier transform method [12] that transfers convolution in one domain to an algebra product in another domain and methods by iterating convolution [13] at every loop to operate de-convolution. A method getting rid of dealing with discrete convolution directly has been discussed [11, 14, 15], which transforms the convolution format to the linear matrix equation in algebra. This method can deal with MRF

✉ Longxiang Li  
leellxhit@126.com

<sup>1</sup> Changchun Institute of Optics, Fine Mechanics and Physics, Chinese Academy of Sciences, Changchun, Jilin 130033, China

<sup>2</sup> University of Chinese Academy of Sciences, Beijing 100049, China

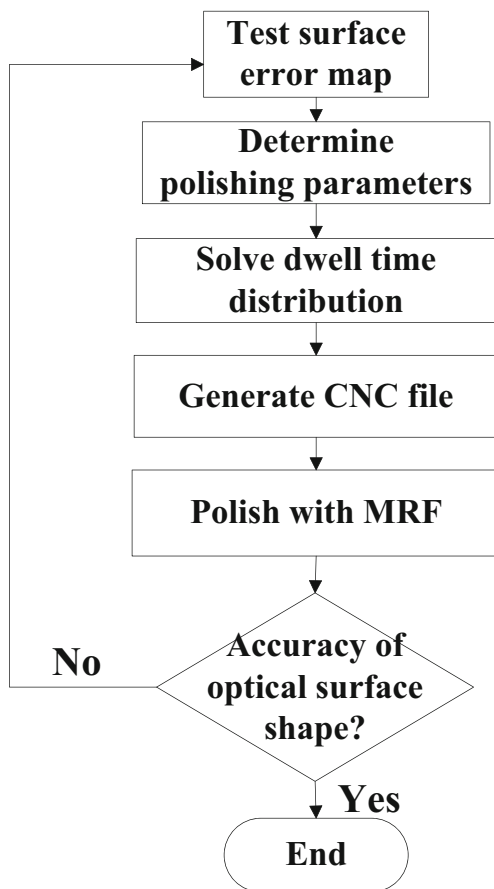


**Fig. 1** Flow chart of MRF

easily for any scanning paths. In addition, this method allows that space densities of dwell points and discrete data of a surface error map are not restricted to the same values and it provides the possibility that variant removal functions or different kinds of scanning paths are used in just one fabricating process. However, because the projected area of MRF's removal function is usually smaller than the pitch lap and SL on the same optical surface of large size, the large quantity of the data of the MRF process and its D-shape removal function challenge the precision and computing rate of the dwell time algorithm. In fact, for MRF, Song et.al [15] have mentioned the dwell time algorithm; however, its computing rate and accuracy are limited, in particular for large data volumes of large optics, and the spiky edge with an oscillation-like wave on the residual surface error map is not taken into account.

Thus, in this paper, the method based on a linear matrix equation is studied in order to establish a reliable dwell time algorithm for MRF, which is faster and more accurate with high convergence efficiency, especially for large optics. Then, a general surface error map extension is developed to retrain the spiky edge with an oscillation-like water wave on the residual surface error map and, at last, an experiment of fabrication is conducted to prove the validity of the algorithm. In Section 2, the MRF device and its removal function by

experimental test are introduced, and the process of building the dwell time matrix equation model is shown. In Section 3, an optimized calculation process of the dwell time including the constrained generalized minimal residual (GMRES) model and adaptive Tikhonov regulation are studied in detail. In Section 4, a general surface error map extension method based on the conformal mapping theory is established. At last, in Section 6, results of simulation and experiments are presented.

## 2 Dwell time matrix equation

### 2.1 MRF removal function

The MRF machine has been developed, cooperating with a team of Belarus, based on a permanent magnet shown in Fig. 2. The components of the MRF device include a magnetorheological fluid cycle system, a working wheel whose diameter is 160 mm in Fig. 2, and a permanent magnet providing a magnetic field in the working area.

The removal function means the distribution of the material removing rate when the wheel works at just one fixed spot on an optical surface. The removal function of the permanent magnet MRF is also the D-shape, just like the MRF based on the electro-magnet. A special type of magnetorheological fluid with 0.5  $\mu\text{m}$  diamond powder is developed for an optical mirror of RB-SiC material, and Fig. 3 presents an example of the removal function produced by the permanent magnet device of MRF. Obviously, the D-shape removal function is symmetric with the  $y$  axis. The peak to valley (PV) of the removal function is 1589.8 nm/min for the RB-SiC material. The parameters are that (a) the wheel rotation rate is 120 r/min, (b) the polishing distance which means the gap between the wheel and the workpiece surface is 1.2 mm, and (c) the flow rate of the magnetorheological fluid is 1 l/min.

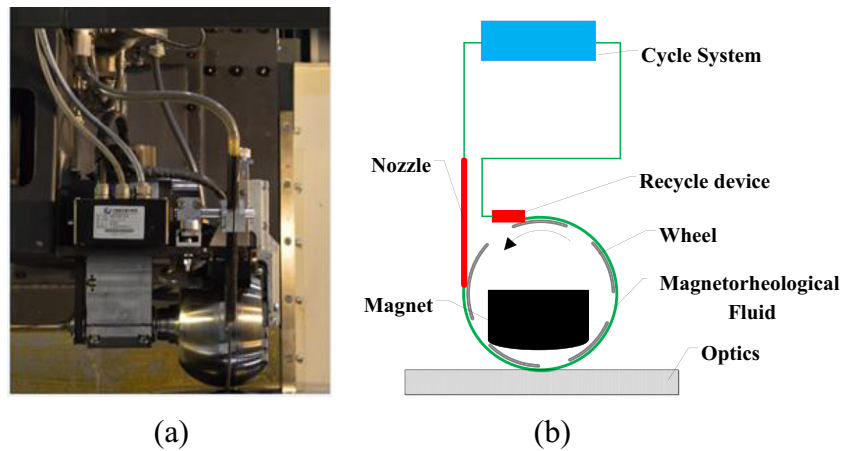
### 2.2 Dwell time matrix equation

MRF inherited the basic characteristics of sub-aperture polishing from the general computer-controlled optical surfacing (CCOS). When the magnetorheological fluid ribbon scans all the dwell points through the fabricating path on an optical surface, the total removal amount  $E(x_i, y_i)$  at some point  $(x_i, y_i)$  can be described as follows.

$$E(x_i, y_i) = \sum_{j=1}^N R(x_i - \xi_j, y_i - \eta_j) \cdot T(\xi_j, \eta_j) \quad (1)$$

$T(\xi_j, \eta_j)$  is the specific period of dwell time at dwell point  $(\xi_j, \eta_j)$ . The total number of dwell points is  $N$ .  $R(x_i - \xi_j, y_i - \eta_j)$  is the material removal amount at data point  $(x_i, y_i)$  on the surface error map when the magnetorheological fluid ribbon dwells

**Fig. 2** The MRF device. **a** MRF machine picture, **b** details of components



on the point  $(\xi_j, \eta_j)$ . The sum format of Eq. (1) can be treated as the 2-D convolution in algebra generally, but it is difficult to deal with the convolution directly in MRF. As to the spiral path on the optical surface, for example, the angle of the D-shape removal function relative to a certain coordinate axis is variable when the ribbon dwells on different points, and the conventional de-convolution method for the circular symmetrical removal function, which is neither Fourier transformation nor the iterative convolution strategy, is applied to this situation.

Indeed, the matrix product can be obtained as shown in Eq. (3) from Eq. (1) with the help of

$$E(x_i, y_i) = e_i, R(x_i - \xi_j, y_i - \eta_j) = r_{ij}, T(\xi_j, \eta_j) = t_j \quad (2)$$

$$\begin{bmatrix} e_1 \\ e_2 \\ \vdots \\ e_M \end{bmatrix} = \begin{bmatrix} r_{11} & r_{12} & \cdots & r_{1N} \\ r_{21} & r_{22} & \cdots & r_{2N} \\ \vdots & \vdots & \ddots & \vdots \\ r_{M1} & r_{M2} & \cdots & r_{MN} \end{bmatrix} \times \begin{bmatrix} t_1 \\ t_2 \\ \vdots \\ t_N \end{bmatrix} \quad (3)$$

$N$  is the total number of dwell points as in Eq. (1), and  $M$  is the total number of the data points from a discrete optical surface map. Obviously, a matrix product in algebra replaces the 2-D convolution. This dwell time computing strategy owns many advantages. It may be applied to almost any type of path that the MRF ribbon scans over, and the space density of the dwell points or data points can be any value which is suitable to grind or polish optical surface, and it provides the possibility that variant removal functions or different types of scanning paths may be used in just one fabricating process as mentioned above. Therefore, this dwell time computing strategy has a wide application in MRF. With the help of

$$e = \begin{bmatrix} e_1 \\ e_2 \\ \vdots \\ e_M \end{bmatrix}, t = \begin{bmatrix} t_1 \\ t_2 \\ \vdots \\ t_N \end{bmatrix}, R = \begin{bmatrix} r_{11} & r_{12} & \cdots & r_{1N} \\ r_{21} & r_{22} & \cdots & r_{2N} \\ \vdots & \vdots & \ddots & \vdots \\ r_{M1} & r_{M2} & \cdots & r_{MN} \end{bmatrix} \quad (4)$$

Eq. (3) can be expressed as

$$Rt = e, t \geq 0 \quad (5)$$

$R$  can be called the removal function matrix in Eq. (5),  $e$  is the initial surface error distribution on the optical surface, and  $t$  is the period of dwell time distributed at different dwell points.

### 3 Optimized non-negative least-squares method

In the MRF process, the removal function matrix whose rows and columns correspond to the number of data points and dwell points, respectively, is usually a large sparse matrix, especially for large optical surfaces. Thus, the calculation process rate, the final precision of the residual surface error, and the stability of the dwell time which is just the solution of Eq. (5) are both needed to be studied in particular.

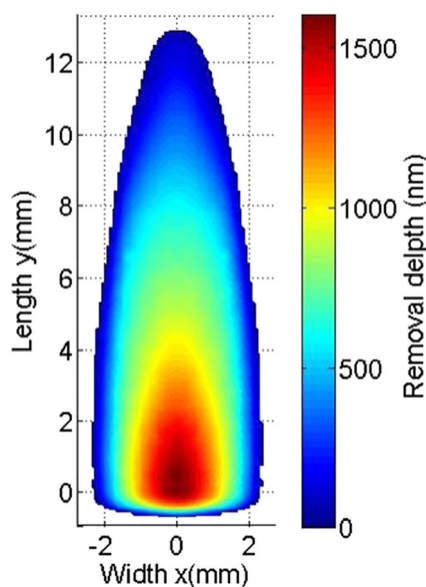


**Fig. 3** MRF removal function distribution

### 3.1 The generalized minimal residual method with non-negative constraint

According to Eq. (5), the process to obtain the dwell time is a typical non-negative least-squares (NNLS) problem in mathematics. With the aim of solving Eq. (5), the format of the dwell time NNLS problem is presented as

$$\underset{t}{\text{minimize}} \quad f(t) = \frac{1}{2} \|Rt - e\|^2, t \geq 0 \quad (6)$$

Equation (6), in fact, optimizes the *root mean square* (RMS) of the residual surface error distribution of the optics to be minimal.

There are many algorithms to deal with Eq. (5), in order to obtain the non-negative solution. For example, in MATLAB software which can be easily achieved, the *fnls* function [16] which is modified based on the Lawson-Hanson algorithm [17] is specialized to solve Eq. (5). However, the computing rate is too slow although *fnls* is faster than the original *lsqnonneg* function in MATLAB.

Many least-squares methods without non-negative constraints own a high rate and accuracy for large linear matrix equations. The generalized minimal residual method (GMRES) is a typically fast projection method for solving linear systems [18] based on the Krylov subspace method. In [18], Yousef Saad gives the details of this method and its improvement. Without considering the non-negative constraints, the solution of Eq. (5) can be solved by GMRES, and the least-squares solution is  $t_{gmr}$ . Apparently,  $t_{gmr}$  usually contains both negative and non-negative elements, but in real application, the dwell time cannot be negative. Thus, the negative elements can be set as zeros directly to obtain the non-negative dwell time distribution  $t_{ngmr}$ .

$$t_{ngmr} = \begin{cases} t_{gmr}, & \text{if } t_{gmr} \geq 0 \\ 0, & \text{if } t_{gmr} < 0 \end{cases} \quad (7)$$

### 3.2 Adaptive Tikhonov regulation

The constrained GMRES method (CGMRES) mentioned above has two problems. The first one is that the residual surface error is so terrible for the MRF process if negative elements are set to zero directly. And the second one is that the dwell time distribution will be sensitive to the noise of initial surface error distribution  $e$ , resulting from environment temperature fluctuation, mechanical vibration, interferometer error, and so on, which cannot be avoided during the measurement process. From the view of algebra, Eq. (5) is a typical discretization of a linear inverse problem which generally gives rise to ill-conditioned linear systems with an ill-conditioned matrix  $R$  of ill-determined rank in MRF. Knowledge in algebra has proved that the stability or sensitivity of

the dwell time to the noise of initial surface error depends on the ill-conditioned degree of matrix  $R$ , that is, the more ill-conditioned  $R$  is, the more unstable the dwell time solution will be. In fact, even though a high precise residual surface correctness is obtained by the slow non-negative method such as *fnls*, the stability of the dwell time is still a problem.

To guarantee the precision of the residual surface shape correctness and the dwell time's stability, an adaptive Tikhonov regulation (ATR) [19–21] is introduced.

With the help of regularization parameter  $\beta$ , Eq. (5) can be expressed as

$$(R^T R + \beta I)t = R^T e, t \geq 0 \quad (8)$$

The optimized goal is

$$\underset{t}{\text{minimize}} \quad f(t) = \left[ \|Rt - e\|^2 + \beta \|It\|^2 \right], t \geq 0 \quad (9)$$

In algebra, the introduction of the regularization parameter  $\beta$  plays a key role in stabilizing the solution of dwell time. The larger  $\beta$  is, the more stable the dwell time is; however, the greater the departure from the real MRF process will be. The converse is true. On the other side, in MRF, the regularization parameter  $\beta$  has a physical meaning. According to Eq. (9),  $\beta$  plays a significant role in trade-off between the period of fabricating time which is exactly the total dwell time and the residual surface error. An adequate beta means a shorter total dwell time and less residual surface errors. The regularization parameter  $\beta$  is usually achieved by the mature L-curve method [22, 23], but its time-consuming property cannot satisfy the demand for MRF with regard to the calculation rate.

With any initial value of beta, the adaptive Tikhonov regulation always regulates beta close to the perfect value by iteration in accordance with Eq. (10). Although the final value of  $\beta$  is not perfect, it is suitable to find a dwell time solution for MRF.

$$\beta^{k+1} = \ln \left( \frac{\|e - Rt_{ngmr}^k\|_2^2}{\|t_{ngmr}^k\|_2^2} + 1 \right) \quad (10)$$

where  $\beta^{k+1}$  is the  $(k+1)$ th modified regularization parameter,  $t_{ngmr}^k$  is the dwell time solution by the constrained GMRES according to Eq. (7) in the  $k$ th iteration. When the difference of solutions between two consecutive iterative cycles is small enough, the iteration is stopped (see Eq. (11)).

$$\frac{\left( \|t_{ngmr}^{k+1}\|_2^2 - \|t_{ngmr}^k\|_2^2 \right)}{\|t_{ngmr}^k\|_2^2} \leq \delta, \delta \geq 0 \quad (11)$$

The combination of CGMRES and adaptive Tikhonov regulation with only several iterations to stopping the criterion in real application not only insures the calculating rate and the

accuracy of residual surface shape correctness but also guarantees the stability of dwell time. The advantages of this method are in solving the dwell time distribution of large optical surfaces.

### 4 General surface error map extension

#### 4.1 Initial surface error

The dwell time algorithm mentioned above has seen a success in MRF, but simulation shows that the residual error at the edge is larger than that within the inner diameter of the optical surface, even though the edge effect of the removal function is considered. The residual error at the edge area has a spiky shape usually with oscillation like a water wave. In fact, in the image restoration, this phenomenon is named as ringing effect [24]. The main reason is that the discontinuity of the surface error at the edge of optics results in incomplete convolution. Since the MRF ribbon can walk out of the optical surface unlike stressed lap or traditional pitch lap, it provides a possibility to retrain the ringing effect at the edge area by considering changes of removal function at the edge area.

One of the possibilities solving the problem above is to extend the initial surface error. Because the optical surface is to be continuous in curvature, the joint area of the surface error map must be smooth and continuous, which means it is continuously derivable in mathematics. The optical surface error

map may be of any shape including square, rectangle with rounded corner, circle, ellipse, and sector. Common extended methods in image restoration, such as periodic extension, symmetrical extension, zero-fill extension, edge filtering, and usual extrapolation, cannot meet the above demands. In [11], the 2-D Gerchberg extension is a proper method but it needs some time to run many iterations in order to get a continuously extended surface.

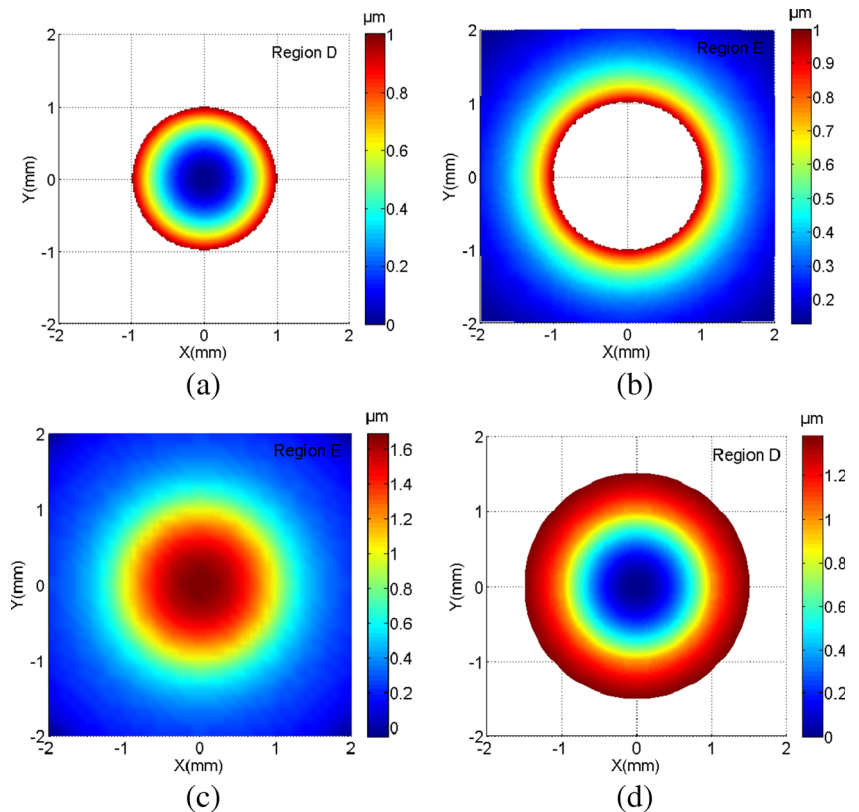
Thus, a fast general surface error map extension method is developed, which is meaningful not only to MRF, but also to IBF and other means that can walk out of the optical surface in optical fabrication processes.

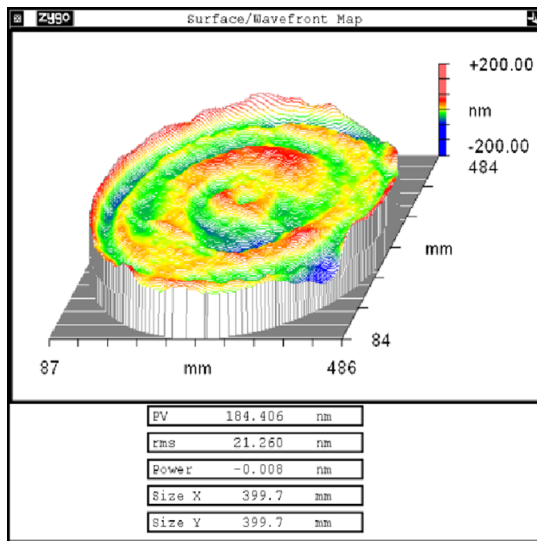
#### 4.2 Conformal mapping process

A conformal mapping process based on the conformal mapping theory [25] in complex variable methods was developed to extend the surface error map, by which an extrapolation is translated to an interpolation. Given a region of  $D$  whose coordinate is  $(x, y)$  on the complex  $z$ -plane in accordance with complex analysis and  $f: w=f(z)$ , where function  $f$  is a fractional function, is a conformal map of  $D$  onto another region  $E$  whose coordinate is  $(u, v)$  of the complex  $w$  plane; the two planes have the relationship

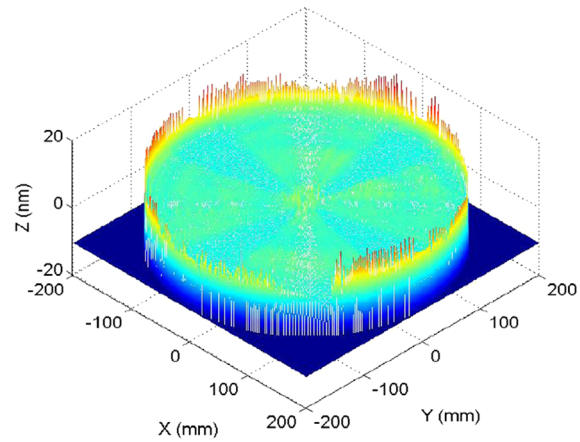
$$\begin{cases} z = x + iy \\ w = u + iv \end{cases} \tag{12}$$

**Fig. 4** Extension based on conformal mapping. **a** The initial surface error map in region D, **b** transformed map in region E, **c** map with Biharmonic Spline Interpolation in region E, **d** inverse transformation onto region D





(a)



(b)

**Fig. 5** The  $\Phi 400$ -mm optics. **a** The initial surface error map, **b** the residual surface error map without extension

$$\begin{cases} u = u(x, y) \\ v = v(x, y) \end{cases} \text{ or } \begin{cases} x = x(u, v) \\ y = y(u, v) \end{cases} \quad (13)$$

Considering the constraints of 2-D extrapolation in map extension in image processing, the 2-D interpolation is much easier by the information from other surrounded points. To reach this goal, Eq. (14) can be devised.

$$w = \frac{1}{z} \quad (14)$$

Thus, the relationship of the coordinates is

$$\begin{cases} u = \frac{x}{x^2 + y^2} \\ v = \frac{-y}{x^2 + y^2} \end{cases} \quad (15)$$

Figure 4a, b presents an example of the process mentioned above. In fact, with the transformation based on Eq. (15), the discrete data points are distributed in the infinite area, but most of the data points concentrate in the area not far from the center in region E. Thus, data points in the limited area are chosen for interpolation as shown in Fig. 4b.

By the Biharmonic Spline Interpolation [26], an extended continuous map is built in region E as shown in Fig. 4c. Then, an inverse transformation of coordinates is necessary with Eq. (16) to obtain the extended surface error map in the original region D as shown in Fig. 4d.

$$\begin{cases} x = \frac{u}{u^2 + v^2} \\ y = \frac{-v}{u^2 + v^2} \end{cases} \quad (16)$$

This method combining conformal mapping with a proper interpolation can be widely used in extension of any shape of image as long as regions are connected, and also it needs less calculated quantities. In the field of the optical fabrication, arbitrary shape regions of the optical surface maps can be extended by this method and this is the reason why it is called a general surface error map extension.

### 5 Simulation and experiment

Simulations and experiments were conducted to demonstrate their advantages and validity of the algorithm in this paper.

**Table 1** The testing results of the CGMRES plus ATR

Diameter/ mm	R dimension		Computing rate/s	$\beta$	PV/nm	RMS/nm
	M	N				
100	7736	11,720	4.18	0.310	63.90	3.71
200	30,921	38,763	10.91	0.081	36.82	1.49
300	69,691	81,513	20.68	0.070	29.95	1.37
400	123,817	139,971	38.47	0.075	27.28	1.29
500	193,694	214,137	65.44	0.068	26.44	1.26

**Table 2** The testing results of the L-curve and *fnnls*

Diameter/mm	Computing rate/s		$\beta$	PV/nm	RMS/nm
	L-curve	<i>fnnls</i>			
100	676.57	1130.31	0.152	52.65	3.45
200	3450.51	5332.82	0.043	34.32	1.34
300	8281.21	12,068.26	0.041	30.83	1.32
400	18,218.68	18,706.03	0.039	26.12	1.29
500	29,149.88	26,288.64	0.038	25.73	1.26

### 5.1 Simulation test for differently scaled optics

First of all, the computing rate and the accuracy of the algorithm of CGMRES with ATR are proved with a small removal function produced by the working wheel whose diameter is 160 mm. Its spot size is about 5 mm×15 mm as shown in Fig. 3. The real basic optical surface is a circle RB-SiC mirror with  $\varphi$ 400 mm diameter in Fig. 5a, which is expanded or compressed by adjusting values of pixel resolution to different scales that are  $\varphi$ 100,  $\varphi$ 200,  $\varphi$ 300, and  $\varphi$ 500 mm, and then, the value of pixel resolution that is just distanced between adjacent data points is kept as 1 mm/pixel by interpolation. Thus, the values of surface shape accuracy are kept almost the same as PV 179.125 nm and RMS 21.26 nm. In the virtual simulation, the spiral path is adopted and the space density of dwell points and data points is nearly the same. In addition, the edge effect of the removal function at the leading edge is taken into account [27]. The algorithm of CGMRES with ATR is implemented by MATLAB-2010b in the Windows system PC with Intel Eight-Core i3 3 GHz CPUs and 16 GB memory.

The testing result of the CGMRES plus ATR is presented in Table 1. With the increase of the scale of optical surfaces, the number of surface data points ( $M$ ) and dwell points ( $N$ ) rises rapidly.  $N$  is a little larger than  $M$  since the MRF removal function always dwells outside of the optics. Computing rate means the time consumed in solving Eq. (5) by algorithm of CGMRES plus ATR. Approximately 1 min is taken by the PC whose specifications are not particular in industry application, while sparse  $R$  dimension is up to 200,000×200,000 for optics of  $\varphi$ 500 mm. The ultimate shape accuracy of differently

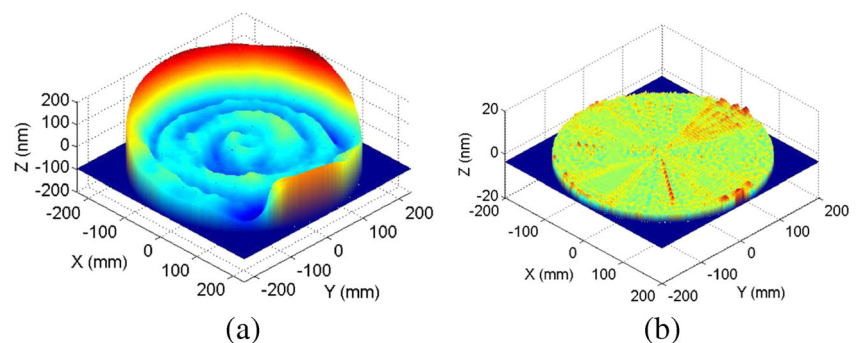
scaled surfaces is enough in real application although the PV and RMS of  $\varphi$ 100 mm surface are not so good, which exactly proves that the space frequency of the surface error map plays a significant role in convergence of optical fabrication processes. In fact, many other available algorithms have been studied, and Table 2 gives testing results based on MATLAB with the same PC. To compare with CGMRES plus ATR, the termination tolerance and iterative maximum number of L-curve and *fnnls* are modified to guarantee accuracy with high computing rate. The PV and RMS of L-curve and *fnnls* are almost the same with those of CGMRES plus ATR; however, the time of L-curve and *fnnls* is much longer. To the  $\varphi$ 100 mm optics, computing time of L-curve and *fnnls* is up to about half an hour comparing with several seconds of CGMRES plus ATR, and when it comes to  $\varphi$ 500 mm optics, about 15 h have to face with the challenge of just about 1 min. Also, anyone cannot ignore the regularization parameter  $\beta$  in Table 1 and Table 2. The  $\beta$  of CGMRES plus ATR is generally less than that of L-curve, but the values are very near for equally scaled optics to ensure the stability of dwell time solutions. Thus, in a summary, the dwell time algorithm of CGMRES plus ATR provides an extremely fast computing process with high accuracy and stability in MRF.

The point necessary to emphasize is that CGMRES plus ATR is also suitable to larger optics, just like 1 m scale or larger. On one hand, for larger optics, the bigger working wheels will be used, such as diameter 200 and 370 mm wheels provided by QED, and as a result, the space density of dwell points and data points can be sparser and the  $R$  dimension will not be much larger. On the other hand, although  $R$  dimension becomes larger, the combined method is predicted to maintain its computing rate and accuracy in a content degree according to Table 1.

### 5.2 Ultimate residual surface error of simulation

Evaluating the residual surface error not only depends on the values of PV and RMS but also on the error distribution of the surface map. General surface error map extension is used to restrain the ring effect of the surface edge shown in Fig. 5b. The surface is extended smoothly and continuously with the 2 time length of MRF removal function shown in Fig. 6a. Then

**Fig. 6** The simulation with surface extension. **a** The initial surface with extension, **b** the residual surface error map of  $\varphi$ 400 mm



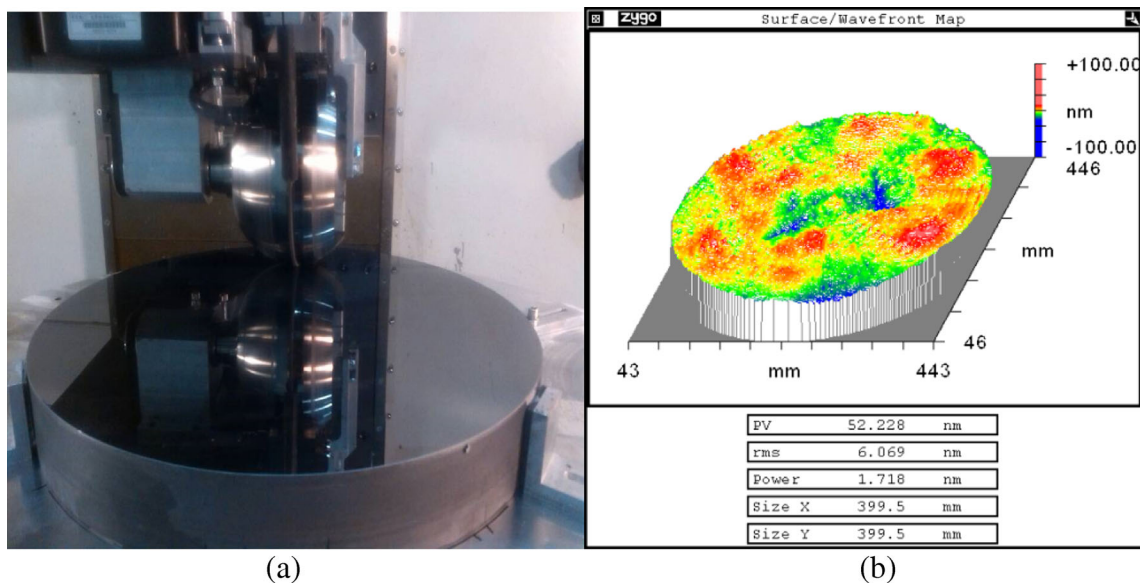


**Fig. 7** Experiment of fabrication. **a** The fabricating process, **b** the final surface error

a virtual fabrication is simulated to the extended surface by considering the edge effect at the leading edge. The sub-aperture residual error map that we needed was measured as shown in Fig. 6b. Obviously, the residual error of the edge is smooth just like inner parts without spiky shape and its oscillation like a water wave. At the same time, the values of PV and RMS reach 7.56 and 0.632 nm, respectively, which are less contrasted with that of diameter 400 mm in Table 1. Thus, introducing general surface error map extension not only restrains the ring effect of the surface edge effectively but also optimizes the values of PV and RMS of the whole surface error map. Because the outer dwell time beyond one time length of removal function has no influence on the factual initial surface error part, it can be abandoned in the real fabricating process.

### 5.3 Experiment

In the experiment, the  $\varphi 400$ -mm plane RB-SiC mirror mentioned in Section 5.1 was processed. Figure 7a shows the fabricating process with the  $\varphi 160$ -mm wheel. After 9.5 h of just one cycle, the result is that the PV and RMS of the  $\varphi 400$  mm mirror is finally 52.23 nm and 6.069 nm, respectively, and the edge is consistent with the other parts on the mirror in Fig. 7b. Compared to the simulated result in Fig. 6b, the actual residual error is larger. Many reasons of the departure between the simulated and actual result are analyzed: (a) the testing precision is crucial, which is often affected by many elements in the lab including environment vibration and atmosphere disturbance, (b) simulation is based on the discrete fixed dwell points which, however, are scanned continuously in real fabricating process, (c) the material homogeneity of RB-SiC of this mirror is a role which cannot be ignored and (d) the removal function

distribution of MRF is not absolutely stable and the experimental testing of removal function distribution is repeated with some little arbitrary error every time. Although the departure exists, the experimental result has proved the validity of the optimized algorithm in this paper.

## 6 Conclusions

Based on the non-circular-symmetrical removal function in MRF, the de-convolution format of dwell time algorithm is transformed to a linear matrix equation. Then, a non-negative least-squares method of CGMRES combined with the adaptive Tikhonov regulation is studied to ensure the accuracy and stability of dwell time solution as well as a much faster computing rate. Finally, by developing the general surface error map extension, a more accurate optical surface is obtained. The simulation for optical surfaces of different diameters showed that CGMRES with adaptive Tikhonov regulation can deal with the dwell time within several minutes with high accuracy and stability, which is much faster than the easily available common method. The PV and RMS of simulated fabrication for  $\varphi 400$  mm converge from 184.41 and 21.26 to 27.28 and 1.29 nm, and ultimately to 7.56 and 0.632 nm with the help of the map extension. Finally, the good results of the fabricating experiment prove the validity of the optimized algorithm. In conclusion, an effective dwell time of MRF can be fast obtained by the algorithm of CGMRES plus adaptive Tikhonov regulation with the general surface error map extension. Moreover, this algorithm not only instructs MRF process effectively but also could be widely applied for other computer control optical surfacing processes.

**Acknowledgments** We acknowledge the National Natural Science Foundation of China (NSFC) for their financial support for projects 61036015 and 2011CB013205.

## References

- Harris DC (2011) History of magnetorheological finishing. *Proc SPIE* 8016(4):561–566
- Das M, Jain VK, Ghoshdastidar PS (2012) Nanofinishing of flat workpieces using rotational–magnetorheological abrasive flow finishing (R-MRAFF) process. *Int J Adv Manuf Technol* 62(1–4):405–420
- Jha S, Jain VK (2009) Rheological characterization of magnetorheological polishing fluid for MRAFF. *Int J Adv Manuf Technol* 42(7–8):656–668
- Bai Z, Yan Q, Lu J, Xu X (2014) Parametric investigation into accommodate-sinking effect of cluster magnetorheological effect pad. *Int J Adv Manuf Technol* 75(9–12):1447–1456
- Shorey AB, Kordonski W, Tricard M (2004) Magnetorheological finishing of large and lightweight optics. *Proc SPIE* 533:99–107
- Schinhaerl M, Schneider F, Rascher R, Vogt C, Sperber P (2010) Relationship between influence function accuracy and polishing quality in magnetorheological finishing. *Proc SPIE* 76550Y-76550Y-76510
- Wang J, Chen W, Han F (2014) Study on the magnetorheological finishing method for the WEDMed pierced die cavity. *Int J Adv Manuf Technol*. (Published online)
- Li H, Zhang W, Yu G (2009) Study of weighted space deconvolution algorithm in computer controlled optical surfacing formation. *Chin Opt Lett* 7(7):627–631
- Luo X, Zheng L, Zhang X (2011) Finite element analysis simulation and experimental verification of the stressed lap's deformation accuracy. *Appl Opt* 50(5):782–787
- Deng H, Ueda M, Yamamura K (2014) Characterization of 4H-SiC (0001) surface processed by plasma-assisted polishing. *Int J Adv Manuf Technol* 72(1–4):1–7
- Wu JF, Lu ZW, Zhang HX, Wang TS (2009) Dwell time algorithm in ion beam figuring. *Appl Opt* 48(20):3930–3937
- Wilson S, McNeil J (1987) Neutral ion beam figuring of large optical surfaces. *Proc SPIE* 818:320–324
- Jones RA (1977) Optimization of computer controlled polishing. *Appl Opt* 16(1):218–224
- Carnal CL, Egert CM, Hylton KW (1992) Advanced matrix-based algorithm for ion-beam milling of optical components. *Proc SPIE* 1752:54–62
- Song C, Dai Y, Peng X (2010) Model and algorithm based on accurate realization of dwell time in magnetorheological finishing. *Appl Opt* 49(19):3676–3683
- Bro R, De Jong S (1997) A fast non-negativity-constrained least squares algorithm. *J Chemom* 11(5):393–401
- Lawson CL, Hanson RJ (1974) Solving least squares problems. Prentice-Hall Series in Automatic Computation
- Iterative methods for sparse linear systems, 2nd, Society for Industrial and Applied Mathematics, Philadelphia, 2003
- Deng WJ, Zheng LG, Shi YL, Wang XK, Zhang XJ (2007) Dwell time algorithm based on matrix algebra and regularization method. *Opt Precis Eng* 15(7):1009–1015 (**in Chinese**)
- Li LX, Deng WJ, Zhang BZ, Bai Y, Zheng LG, Zhang XJ (2014) Dwell time algorithm for large optics in magnetorheological finishing. *Acta Opt Sin* 31(5):0522001 (**in Chinese**)
- Lee ES, Kang MG (2003) Regularized adaptive high-resolution image reconstruction considering inaccurate subpixel registration. *IEEE Trans Image Process* 12(7):826–837
- Hansen PC, O'Leary DP (1993) The use of the L-curve in the regularization of discrete ill-posed problems. *SIAM J Sci Comput* 14(6):1487–1503
- Calvetti D, Morigi S, Reichel L, Sgallari F (2000) Tikhonov regularization and the L-curve for large discrete ill-posed problems. *J Comput Appl Math* 123(1):423–446
- Andrews HC, Hunt BR (1977) Digital image restoration. Prentice-Hall, Englewood Cliffs New Jersey
- Baricco GA, Olivero AM, Rodríguez EJ, Safar FG, Sanz JL (1995) Conformal mapping-based image processing: theory and applications. *J Vis Commun Image Represent* 6(1):35–51
- Sandwell DT (1987) Biharmonic spline interpolation of GEOS-3 and SEASAT altimeter data. *Geophys Res Lett* 14(2):139–142
- Hu H, Dai Y, Peng X, Wang J (2011) Research on reducing the edge effect in magnetorheological finishing. *Appl Opt* 50(9):1220–1226